Chirality-enhanced nonlinear optical response of frustrated liquid crystals

Guilhem Poy[a] and Slobodan Žumer[b,a]

[a]Faculty of Mathematics and Physics, University of Ljubljana, Jadranska 19, 1000 Ljubljana, Slovenia
[b]Jožef Stefan Institute, Jamova cesta 39, 1000 Ljubljana, Slovenia

Guilhem Poy, Slobodan Žumer, "Chirality-enhanced nonlinear optical response of frustrated liquid crystals", Proc. SPIE 11807, Liquid Crystals XXV, 1180708 (September 2, 2021). DOI: http://dx.doi.org/10.1117/12.2593920.

ABSTRACT

Liquid crystals (LCs) are known to have a facile response under external electric and optical fields, which in the past have led to various technological applications such as LC displays or self-focusing flat lenses. In this contribution, we describe how chirality can increase the overall nonlinear optical response of frustrated liquid crystal samples based on the formalism of Green functions. We describe how such an effect can be leveraged to generate low-power spatial optical solitons, and also suggest possible experiments that could be derived from this theoretical and numerical work.

Keywords: Liquid crystals, spatial optical solitons, chirality

1. INTRODUCTION

A nematic liquid crystal (LC) is a mesophase associated with orientational order, with the mean orientation of molecules at a given point called the director $\boldsymbol{n}$. The strong response of this phase to external fields and its intrinsic birefringence have allowed numerous optical applications, such as the LC displays widely used in TVs, phones, laptops and desktop monitors. Interestingly, the optical field carried by a sufficiently powerful light beam can induce a reorientation of the director $\boldsymbol{n}$ and therefore an effective modulation of the permittivity tensor of the LC that lead to various nonlinear optical effects. Perhaps the most fascinating of these effects is the emergence of spatial optical solitons at powers as low as ~ 1 mW propagating in the central plane of uniformly-aligned nematic layers. These optical solitons correspond to self-focused beams for which the optically-induced perturbation of the permittivity exactly compensates the natural diffraction of light fields, thus allowing the transverse amplitude profile of the beam to be preserved as it propagates. These solitons were first observed in the 2000s by the groups of Karpierz[1] and Assanto,[2] and were dubbed *nematicons* when the light's polarisation and wavevector and the LC's director are all in the same plane.

Many studies extended the seminal works of Assanto and Karpierz during the past 20 years, showing that spatial optical solitons in LCs are robust carrier of optical information which, contrary to solitons in Kerr media, are not subject to catastrophic collapse of the beam thanks to the nonlocal response of the liquid crystal.[3] Optical solitons can be steered in the plane of the sample by tuning the unperturbed director with external fields,[4,5] and they can undergo self-induced mode transformation[6] or exhibit bistability near a first order transition.[7]

Further author information: (Send correspondence to G.P.)
G.P.: guilhem.poy@fmf.uni-lj.si
S.Ž.: slobodan.zumer@fmf.uni-lj.si

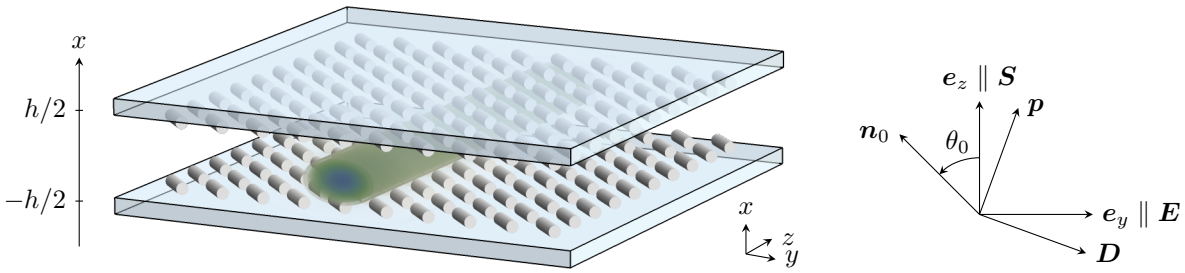

Figure 1. Our system consists of a laser beam (green) propagating in a chiral LC layer confined between two glass plates (blue). The unperturbed director field $\boldsymbol{n}_0$ is imposed by the anchoring potentials on the plates and is in the plane of the sample (yz). The wavevector $\boldsymbol{p}$ is chosen so that the Poynting vector $\boldsymbol{S}$ (resp., the electric field $\boldsymbol{E}$) is parallel to the z-direction (resp., y-direction).

They can also assist random lasing in dye-doped liquid crystals,[8] or interact in highly nontrivial ways with the Pancharatnam-Berry geometric phase of LCs.[9]

In a recent paper,[10] we showed that chirality was playing a major role in the nonlinear optical response of LC samples with homeotropic boundary conditions ($\boldsymbol{n}$ is anchored normally to the confining plates of the sample). By adding chiral molecules to such a sample—thereby obtaining a so-called frustrated cholesteric sample— we experimentally and numerically showed that the overall response of the LC to external fields was boosted by chirality and that periodically self-focused beams with an intricate field pattern bouncing between the plates of the sample could be generated at a lower power than in achiral media. This chirality-enhancement effect was suggested to be a straightforward improvement for the various solitonic effects described above, possibly leading to soliton-based photonics devices with even lower power consumption. However, the particular sample geometry studied in this previous contribution prevented any advanced theoretical analysis because of the associated complicated periodic field patterns, and could not be directly compared to the well-understood case of nematicons (beam propagating parallel to the plates of the sample).

The aim of this paper is to overcome these shortcomings by focusing on a simpler—but still chiral and frustrated—class of LC samples with a far-field director parallel to the confining plates of the sample. In Sec. 2, we present our theoretical approach to model the nonlinear optical propagation of light beam in such samples and explicitly show that chirality is also boosting the nonlinear optical response of these frustrated samples based on the formalism of Green functions. In Sec. 3, we explore how the power of a fundamental soliton vary with the parameters of our system and also present numerical simulations allowing to validate our theoretical approach. Finally, we draw our conclusions in Sec. 4 and suggest a few experiments that could be based on this purely theoretical and numerical work.

2. THEORETICAL MODEL

In this section, we introduce the theoretical equations necessary to model the reorientation of frustrated chiral LC under optical fields and the associated self-focusing effect for the propagation of laser beams. Fig. 1 shows the system considered here, which consists of a cholesteric layer of thickness h confined between two glass plates treated for planar anchoring along the in-sample plane direction $\boldsymbol{n}_0 = \cos\theta_0 \boldsymbol{e}_z - \sin\theta_0 \boldsymbol{e}_y$. When the spontaneous twist $q = 2\pi/P$ of the cholesteric (with P the pitch of the equilibrium cholesteric helix in an unconfined sample) is smaller than a critical value q_c, the fully unwound director field $\boldsymbol{n} = \boldsymbol{n}_0$ is a metastable state of the LC system. The exact expression of q_c will be given later in this section, but we can already note that it has the same order of magnitude as π/h, with h the sample thickness. Note that for intermediate values of spontaneous twist and LCs with standard anisotropy of elastic constants, the π-twisted director field is also a possible metastable state with lower energy than the unwound director field.[11] Here, we assume that the whole sample is always filled with the unwound state, which in experiments can be attained by transitioning the LC sample from the isotropic phase to the cholesteric phase under the action of a strong external field imposing $\boldsymbol{n} = \boldsymbol{n}_0$, and then cutting out the field once the sample is fully transitioned.

When weakly perturbed by an optical field $\boldsymbol{E}$, the director field can be written as $\boldsymbol{n} = \boldsymbol{n}_0 + \boldsymbol{\delta n}$ with $\boldsymbol{\delta n} \perp \boldsymbol{n}_0$ the director field deviation. The latter quantity introduces spatial variations in the permittivity tensor $\boldsymbol{\epsilon}$, which may affect the propagation of the optical field and therefore acts as a source of optical nonlinearity. More specifically, we develop at first order in $\boldsymbol{\delta n}$ the permittivity tensor:

$$\boldsymbol{\epsilon} = \begin{cases} \boldsymbol{\epsilon}^\star + \boldsymbol{\delta\epsilon}, & |x| < h/2 \\ n_p^2 \mathbf{I}, & |x| > h/2 \end{cases} \tag{1}$$

where $\boldsymbol{\epsilon}^\star \equiv n_o^2\mathbf{I} + \left[n_e^2 - n_o^2\right] \boldsymbol{n}_0 \otimes \boldsymbol{n}_0$ is the unperturbed LC permittivity tensor, $\boldsymbol{\delta\epsilon} = \left[n_e^2 - n_o^2\right] \left[\boldsymbol{n}_0 \otimes \boldsymbol{\delta n} + \boldsymbol{\delta n} \otimes \boldsymbol{n}_0\right]$ is the perturbation of permittivity tensor, and n_e, n_o and n_p are the extraordinary, ordinary, and glass plates' refractive indices. In the next two subsections, we derive the coupled differential equations that governs the evolution of $\boldsymbol{\delta n}$ and $\boldsymbol{E}$ in our chiral system.

2.1 Beam propagation equation

We are interested in a laser beam of wavelength λ propagating in the plane of the sample along the z-direction (see Fig. 1). We write the electric field associated with such a beam as $\boldsymbol{E} = \exp\left[ik_0 \boldsymbol{p} \cdot \boldsymbol{r}\right] \boldsymbol{A}$, with $k_0 = 2\pi/\lambda$ the wavevector in empty space, $\boldsymbol{p}$ the renormalized wavevector, and $\boldsymbol{A}$ a slowly-spatially-varying vector amplitude. Since the propagation medium is birefringent, the renormalized wavevector is in general not parallel to the Poynting vector $\boldsymbol{S} \parallel \boldsymbol{e}_z$, and can be shown to be $\boldsymbol{p} = \sqrt{\epsilon_{yy}^\star}\left[\boldsymbol{e}_z - (\epsilon_{yz}^\star/\epsilon_{yy}^\star)\boldsymbol{e}_y\right]$. Starting from the wave equation in anisotropic media as given in Ref.,[12] we obtain after applying the well-known Slowly Varying Envelope Approximation (SVEA) and keeping only leading nonlinear contributions in $\delta\epsilon$:

$$\left\{2ik_0 p_z \left[\partial_z + \nu\partial_y\right] + \mathcal{D}_x\partial_x^2 + \mathcal{D}_y\partial_y^2 + k_0^2\bar{\epsilon}\right\} A_y = 0, \tag{2}$$

where we defined (assuming $n_o \approx n_p$ for simplicity, which is true for the glass plates and liquid crystals considered here):

$$\nu = \begin{cases} 0, & |x| \le h/2 \\ -\epsilon_{yz}^\star/n_p^2, & |x| > h/2 \end{cases} \qquad \bar{\epsilon} = \begin{cases} \delta\epsilon_{yy}, & |x| \le h/2 \\ n_p'^2 - \epsilon_{yy}^\star, & |x| > h/2 \end{cases} \tag{3}$$

$$\mathcal{D}_x = \epsilon_{yy}^\star/n_e^2 \qquad \mathcal{D}_y = \begin{cases} \left[\epsilon_{yy}^\star/(n_e n_o)\right]^2, & |x| \le h/2 \\ p_z^2/(n_p^2 - p_z^2), & |x| > h/2 \end{cases} \tag{4}$$

with $n_p' = \sqrt{n_p^2 - p_y^2 p_z^2/(n_p^2 - p_y^2)}$. Eq. (2) corresponds to the paraxial beam propagation equation for the amplitude A_y. It can be checked to be identical to the one given in Ref.,[13] although our equation is slightly more general since it also includes confinement effects due to the jumps of permittivity at the LC/glass plate interfaces*. This equation is formally equivalent to the Schrödinger equation, with the time replaced by the propagation distance z. The diffraction operator $\mathcal{D}_x\partial_x^2 + \mathcal{D}_y\partial_y^2$ is responsible for the spreading of the transverse amplitude profile of a propagating beam, whereas the permittivity modulation $\bar{\epsilon}$ is formally equivalent to a potential allowing the confinement of the light fields. Note that the other components A_x and A_z of the vector amplitude have amplitudes much smaller than A_y. They can be expressed as a differential operator times A_y at leading order in the SVEA approach:

$$A_x \approx \left[\frac{i(p_y/k_0)\partial_x - \delta\epsilon_{xy}}{\epsilon_{xx} - p_y^2 - p_z^2}\right] A_y \ll A_y, \qquad A_z \approx \left[\frac{i(p_z/k_0)\partial_y - \delta\epsilon_{yz}}{\epsilon_{zz} - p_y^2}\right] A_y \ll A_y. \tag{5}$$

We focus on the regime of strongly confined light in very thin samples, and therefore use a similar approach than Karpierz *et al.*[1] by writing $A_y(x,y,z) = A(y,z)\ \psi^{(m)}(x,z)$, where $\psi^{(m)}$ is the y-polarized waveguide mode

*We also remark that the angle θ_0, which here is defined as the angle between the director and Poynting vector, is defined differently in the aforementioned reference as the angle between the director and wavevector. Our choice leads to considerably simpler expressions for the coefficients involved in the beam propagation equation.

of order m of our system. Its expression in the LC slab can be calculated as:

$$\psi^{(m)}(x,z) = \sin\left[\xi^{(m)}k_0 x - \frac{m\pi}{2}\right]\exp\left\{-\frac{ip_z\left[\xi^{(m)}\right]^2}{2n_e^2}k_0 z\right\}, \tag{6}$$

where the renormalized wavevector $\xi^{(m)}$ is solution of the following transcendental equation[†]:

$$\xi^{(m)}X_c + \sin^{-1}\left(\frac{\xi^{(m)}}{\Delta n}\right) = \frac{m\pi}{2}, \tag{7}$$

with $\Delta n = n_e\sqrt{1-(n_p'/p_z)^2}$ and $X_c = k_0 h/2$. Integrating Eq. (2) times $[\psi^{(m)}]^\star$ over the interval $x \in [-h/2, h/2]$ using the *ansatz* defined above for A_y yields an effective (1+1)D beam propagation equation for the amplitude $A(y,z)$, as in the approach of the Karpierz:[1]

$$\left[2ik_0 p_z\partial_z + \mathcal{D}_y\partial_y^2 + k_0^2\langle\delta\epsilon_{yy}\rangle\right]A = 0, \qquad \text{with } \langle\delta\epsilon_{yy}\rangle \equiv \frac{\int_{-h/2}^{h/2}\delta\epsilon_{yy}\left|\psi^{(m)}\right|^2\mathrm{d}x}{\int_{-h/2}^{h/2}\left|\psi^{(m)}\right|^2\mathrm{d}x}. \tag{8}$$

$\langle\delta\epsilon_{yy}\rangle$ can be interpreted as the x-averaged nonlinear optical response of the LC material, and unlocks the possibility of compensating the diffraction term $\mathcal{D}_y\partial_y^2$ when the beam power is high enough. Our approach, although simplistic, allows us to completely eliminate the diffraction along the x-direction and to focus on what happens to the beam profile in the y-direction, i.e. in the plane of the sample.

2.2 Molecular reorientation equation

The director field deviation can be calculated from the equations of nematoelasticity,[11] by developing at second order in $\boldsymbol{\delta n}$ the total free energy of the system and then minimizing it with respect to $\boldsymbol{\delta n}$. Writing the deviation as $\boldsymbol{\delta n} = n_\perp\boldsymbol{e}_\perp + n_\parallel\boldsymbol{e}_\parallel$, with $\boldsymbol{e}_\parallel \equiv \boldsymbol{n}_0\times\boldsymbol{e}_x$ and $\boldsymbol{e}_\perp \equiv \boldsymbol{e}_\parallel\times\boldsymbol{n}_0$, we obtain:

$$\mathbf{H}\begin{pmatrix}n_\perp\\ n_\parallel\end{pmatrix} = \frac{\epsilon_0\epsilon_a}{2K_1}\Re\begin{pmatrix}\left[\boldsymbol{E}\cdot\boldsymbol{e}_\perp\right]\left[\boldsymbol{E}\cdot\boldsymbol{n}_0\right]^\star\\ \left[\boldsymbol{E}\cdot\boldsymbol{e}_\parallel\right]\left[\boldsymbol{E}\cdot\boldsymbol{n}_0\right]^\star\end{pmatrix}, \tag{9}$$

where $\mathbf{H}$ is a self-adjoint differential operator governing the linear response of the LC under the action of external fields:

$$\mathbf{H} = -\begin{pmatrix}\partial_\perp^2 + \kappa_{21}\partial_\parallel^2 + \kappa_{31}\partial_n^2 & 2q\kappa_{21}\partial_n + (1-\kappa_{21})\partial_\parallel\partial_\perp\\ -2q\kappa_{21}\partial_n + (1-\kappa_{21})\partial_\parallel\partial_\perp & \kappa_{21}\partial_\perp^2 + \partial_\parallel^2 + \kappa_{31}\partial_n^2\end{pmatrix}, \tag{10}$$

with $\partial_\perp \equiv \boldsymbol{e}_\perp\cdot\boldsymbol{\nabla}$, $\partial_\parallel \equiv \boldsymbol{e}_\parallel\cdot\boldsymbol{\nabla}$, $\partial_n \equiv \boldsymbol{n}_0\cdot\boldsymbol{\nabla}$, and $\kappa_{ij} \equiv K_i/K_j$. The constants K_{1-3} corresponds to the usual splay, twist and bend elastic constants of the LC, and ϵ_a is the anisotropy of relative dielectric permittivity evaluated at the frequency of the external field $\boldsymbol{E}$. The deviations $n_\parallel$ and $n_\perp$ are respectively associated with in-sample-plane and out-of-sample-plane molecular reorientations in our particular sample geometry.

As explained above, the unwound state $\boldsymbol{n} = \boldsymbol{n}_0$ is only stable for a finite range of spontaneous twist $q \in [-q_c, q_c]$. The theoretical expression of q_c can be easily calculated by examining the determinant of the operator $\mathbf{H}$ in Fourier space. Indeed, q_c should corresponds to the minimal value of q for which this determinant becomes zero for at least one Fourier mode, which indicates a change of sign of the free energy curvature with respect to perturbations proportional to this particular Fourier mode. Doing this analysis, we find:

$$q_c = \frac{\pi}{h}\left[\frac{1+\sqrt{\kappa_{12}}}{2\sqrt{\kappa_{23}}}\right]. \tag{11}$$

Above this threshold, a periodic unstable mode develops along the direction of $\boldsymbol{n}_0$, associated with a wavevector $q_\parallel = (\pi/h)\left(\kappa_{23}/\kappa_{31}\right)^{1/4}$. To the best of our knowledge, this instability was never observed experimentally,

[†]Note when the mode index m is too big, this equation no longer admits a solution, which of course means that there are only a limited number of waveguide modes.

probably because it is not trivial to stabilize the metastable planar unwound cholesteric when $q > \pi/(2h)$; indeed, since $q_c > \pi/(2h)$ for common liquid crystals with K_2 smaller than $K_{1,3}$, the π-twisted director field will be the lowest energy state of the system when $q \in [\pi/2h, q_c]$.[11] In such a case, localized domains with a π-twist of the director field will grow and eventually completely fill the LC sample, thus completely hiding the transition described above and destroying the unwound state that is at the core of this work. Here, we assume that the potential nucleation of π-twisted domains in a given LC sample was prevented by transitioning the sample from the isotropic phase to the cholesteric phase under the action of a strong field imposing $\boldsymbol{n} = \boldsymbol{n}_0$. We also assume that $|q| < q_c$ so that the unwound director field is always metastable, and will plot our results with respect to the rescaled spontaneous twist q/q_c.

The reorientation equation (9) describes in a very general way the linear response of unwound chiral LC under arbitrary external AC fields $\boldsymbol{E}$, and is actually valid for any director orientation $\boldsymbol{n}_0$ imposed by the boundary plates[‡], where the Dirichlet boundary conditions $n_\parallel = n_\perp = 0$ must be imposed. We now simplify this equation assuming that $\boldsymbol{n}_0$ is the in-sample-plane orientation defined earlier and $\boldsymbol{E}$ corresponds to the optical field described in the last section (in which case ϵ_a is simply $n_e^2 - n_o^2$). Since we are interested in the coupled light-matter equations, we found it very convenient to introduce the so-called photonics potentials associated with the molecular reorientations $n_\parallel$ and $n_\perp$:

$$\Gamma_{\parallel,\perp} \equiv \frac{K_1 c \sqrt{\epsilon^\star_{yy}}}{\epsilon^\star_{yz} P} n_{\parallel,\perp}, \tag{12}$$

where P is the beam power contained inside the LC slab, and can be calculated at leading order in A_y as:

$$P = \frac{\epsilon_0 c \sqrt{\epsilon^\star_{yy}}}{2} \int_{-h/2}^{h/2} \int_{-\infty}^{\infty} |A_y|^2 \, \mathrm{d}x \, \mathrm{d}y. \tag{13}$$

Switching back to the referential xyz for the derivatives and assuming negligible z-derivatives (which is true for a fundamental optical soliton propagating along z, as considered here), we find that Eq. (9) can be rewritten as:

$$\begin{pmatrix} \mathcal{L}(1, \eta_\perp) & q\eta_q \partial_y - \eta_c \partial_x \partial_y \\ -q\eta_q \partial_y - \eta_c \partial_x \partial_y & \mathcal{L}(\kappa_{12}, \eta_\parallel) \end{pmatrix} \begin{pmatrix} \Gamma_\perp \\ \Gamma_\parallel \end{pmatrix} = \begin{pmatrix} 0 \\ \mathcal{J} \end{pmatrix}, \tag{14}$$

where $\mathcal{L}(\eta, \eta') \equiv -\eta \partial_x^2 - \eta' \partial_y^2$ is minus an anisotropic laplacian and $\mathcal{J} \equiv [A_y|^2 / \int_{-h/2}^{h/2} \int_{-\infty}^{\infty} |A_y|^2 \, \mathrm{d}x \, \mathrm{d}y$ is the renormalized intensity profile of the beam. The following elastic anisotropy factors were defined:

$$\eta_\perp = \kappa_{21} \cos^2\theta_0 + \kappa_{31} \sin^2\theta_0, \qquad \eta_\parallel = \cos^2\theta_0 + \kappa_{31} \sin^2\theta_0, \qquad \eta_q = 2\kappa_{21} \sin\theta_0, \qquad \eta_c = (1 - \kappa_{21}) \cos\theta_0. \tag{15}$$

Note that we only kept the leading contribution in A_y when developping the field $\boldsymbol{E}$, neglecting the small A_x and A_z components as in the original approach of Conti *et al.* in achiral media.[13]

2.3 Coupled light-matter equations and Green functions

To summarize, the coupled light-matter equations described in Eqs. (8,14) are:

$$\left[2ik_0 p_z \partial_z + \mathcal{D}_y \partial_y^2 + \frac{2k_0^2 P}{P_0} \Gamma_{\mathrm{eff}} \right] A = 0, \tag{16}$$

$$\mathbf{H} \begin{pmatrix} \Gamma_\perp \\ \Gamma_\parallel \end{pmatrix} = \begin{pmatrix} 0 \\ \mathcal{J} \end{pmatrix}, \tag{17}$$

with $P_0 = K_1 c \sqrt{\epsilon^\star_{yy}} / [\epsilon^\star_{yz}]^2$ a typical power and $\mathbf{H}$ the matrix differential operator on the left-hand-side of Eq. (14). Under this form, the optical non-linearity clearly appears to be proportional to the beam power P and modulated by the effective photonics potential $\Gamma_{\mathrm{eff}} \equiv \langle \Gamma_\parallel \rangle$. Contrary to the classical case of nematicons in

[‡]However, note that the critical spontaneous twist q_c derived here is only valid for in-sample-plane director orientation $\boldsymbol{n}_0$.

achiral media,[13] one must take into account both components of the director field in the reorientation equation since chirality is coupling them in a non-trivial way[§].

To calculate the photonics potential $\Gamma_{\parallel}$, one can formally use the Green function $\mathbf{G}$ of the differential operator $\mathbf{H}$, and more specifically its bottom right component which we denote by $G_{\parallel}$:

$$\Gamma_{\parallel}(x,y) = \int_{-h/2}^{h/2}\int_{-\infty}^{\infty} G_{\parallel}\left(x,x',y-y'\right)\mathcal{J}\left(x',y'\right)\mathrm{d}x'\ \mathrm{d}y'. \tag{18}$$

Note that one cannot assume translational invariance in the x direction because of the boundary conditions $\boldsymbol{n} = \boldsymbol{n}_0$ at the confining plates of the sample. We deduce from the last equation the effective photonics potential:

$$\Gamma_{\mathrm{eff}}(y) = \int_{-\infty}^{\infty} G_{\mathrm{eff}}\left(y-y'\right)\mathcal{J}_{\mathrm{eff}}\left(y'\right)\mathrm{d}y'. \tag{19}$$

where we defined the effective intensity profile in the y-direction $\mathcal{J}_{\mathrm{eff}} \equiv |A|^2/\int |A|^2\mathrm{d}y$ and the effective Green function:

$$G_{\mathrm{eff}}(y) \equiv \frac{\int_{-h/2}^{h/2}\int_{-h/2}^{h/2} G\left(x,x',y\right)\left|\psi^{(m)}(x)\right|^2\left|\psi^{(m)}(x')\right|^2\mathrm{d}x\ \mathrm{d}x'}{\left[\int_{-h/2}^{h/2}\left|\psi^{(m)}(x)\right|^2\mathrm{d}x\right]^2}. \tag{20}$$

Since the y-direction is not confined, one can easily see that $\tilde{\Gamma}_{\mathrm{eff}} = \tilde{G}_{\mathrm{eff}}\tilde{\mathcal{J}}_{\mathrm{eff}}$, where a tilde indicates a Fourier transform over y. The general expression of $\tilde{G}_{\mathrm{eff}}$ is quite complicated, and we refer to the appendix for our approach to calculate it. Here, we will simply remark that the role of chirality in the response of the confined LC can be easily deduced from an approximate expression of $\tilde{G}_{\mathrm{eff}}(q_y)$ (with q_y the Fourier frequency along y) assuming that the LC response along the x-direction can be modeled by a single discrete Fourier mode at frequency $q_x = \pi/h$:

$$\tilde{G}_{\mathrm{eff}}(q_y) \sim \frac{q_x^2 + \eta_{\perp}q_y^2}{\left(q_x^2+\eta_{\parallel}q_y^2\right)\left(\kappa_{21}q_x^2+\eta_{\perp}q_y^2\right) - q^2\eta_q^2q_y^2}. \tag{21}$$

Indeed, this expression directly shows that $\tilde{G}_{\mathrm{eff}}$ increases when q increases, with a possible divergence at the threshold of instability $q = q_c$ described earlier. Therefore, one can expect that chirality is enhancing the nonlinear optical response of the LC, as verified numerically in the next section.

We conclude this section by providing an estimation of the power necessary to generate a fundamental optical soliton. We follow the classical approach presented in the reference book on nematicons edited by Assanto[14] by only keeping the first two terms in the Taylor expansion of the photonics potential in Eq. 16. Intuitively, this is equivalent to saying that the potential Γ_{eff} has a parabolic form allowing to confine the beam, similar to a gradient-index optical fiber. This approach is exact only in the ideal limit of infinite non-locality with a sufficiently regular Green function, but nevertheless provide a reliable estimation of the threshold of creation of optical soliton in our system. Assuming amplitude solutions of the form $A = A_0\exp\left\{-y^2/(2\omega_0^2) + ik_zz\right\}$, we find:

$$\begin{aligned} 0 &\approx \left\{2ik_0p_z\partial_z + \mathcal{D}_y\partial_y^2 + \frac{k_0^2P}{P_0}\left[2\Gamma_{\mathrm{eff}}(0) + \Gamma''_{\mathrm{eff}}(0)y^2\right]\right\}A \\ &= \left\{\left[\frac{2k_0P\Gamma(0)}{P_0} - 2k_0p_zk_z - \frac{\mathcal{D}_y}{\omega_0^2}\right] + \left[\frac{\mathcal{D}_y}{\omega_0^4} + \frac{k_0^2P\Gamma''_{\mathrm{eff}}(0)}{P_0}\right]y^2\right\}A. \end{aligned} \tag{22}$$

The soliton power P and nonlinear correction k_z to the wavevector can be deduced by equating to zero both terms from the last equation. Here, only the soliton power interests us:

$$\frac{P}{P_0} = \frac{\mathcal{D}_y}{k_0^2\omega_0^4\left[-\Gamma''_{\mathrm{eff}}(0)\right]}, \tag{23}$$

[§]Conversely, when $q = 0$, one can fully eliminate $\Gamma_{\perp}$ from the problem and search a solution for $\Gamma_{\parallel}$ with the same symmetry as the intensity profile $\mathcal{J}$.

with:

$$-\Gamma''_{\text{eff}}(0) = \int_{-\infty}^{\infty} q_y^2 \tilde{G}_{\text{eff}}(q_y) \exp\left\{-\left[\frac{q_y \omega_0}{2}\right]^2\right\} \frac{\mathrm{d}q_y}{2\pi}. \tag{24}$$

The last two equations allow a convenient numerical calculation of the fundamental soliton power P for a given beam waist ω_0, elastic anisotropy factors κ_{21} and κ_{23}, far-field director angle θ_0, and rescaled spontaneous twist q/q_c. When $q = 0$ and $\kappa_{21} = \kappa_{23} = 1$, these equations are very similar to the ones given in Refs.[13,14] (with the exception that these references focus more on 2+1 beam propagation with negligible role of the sample plates). In the next section, we examine how the soliton power changes with all the parameters enumerated above, and also give a few examples of numerically calculated solitons with a general numerical scheme that one of us recently introduced.

3. THEORETICAL AND NUMERICAL RESULTS

3.1 Theoretical predictions for the soliton power

To gain insight on how the fundamental soliton power is affected by chirality, sample geometry, and elastic anisotropy, we calculated P using Eqs. (23, 24) for various sets of parameters. Eq. (24) was approximated at a relative precision of 10^{-4} using Mathematica. In all calculations, we used the sample thickness, light wavelength

Table 1. Values of the sample thickness, light wavelength and material constants used in all our calculations. The material constants corresponds to the liquid crystal E7 at room temperature[15,16] and typical crown glasses.[17]

h (μm)	λ (μm)	K_1 (pN)	n_e	n_o	n_p
2	0.5	11	1.746	1.522	1.51

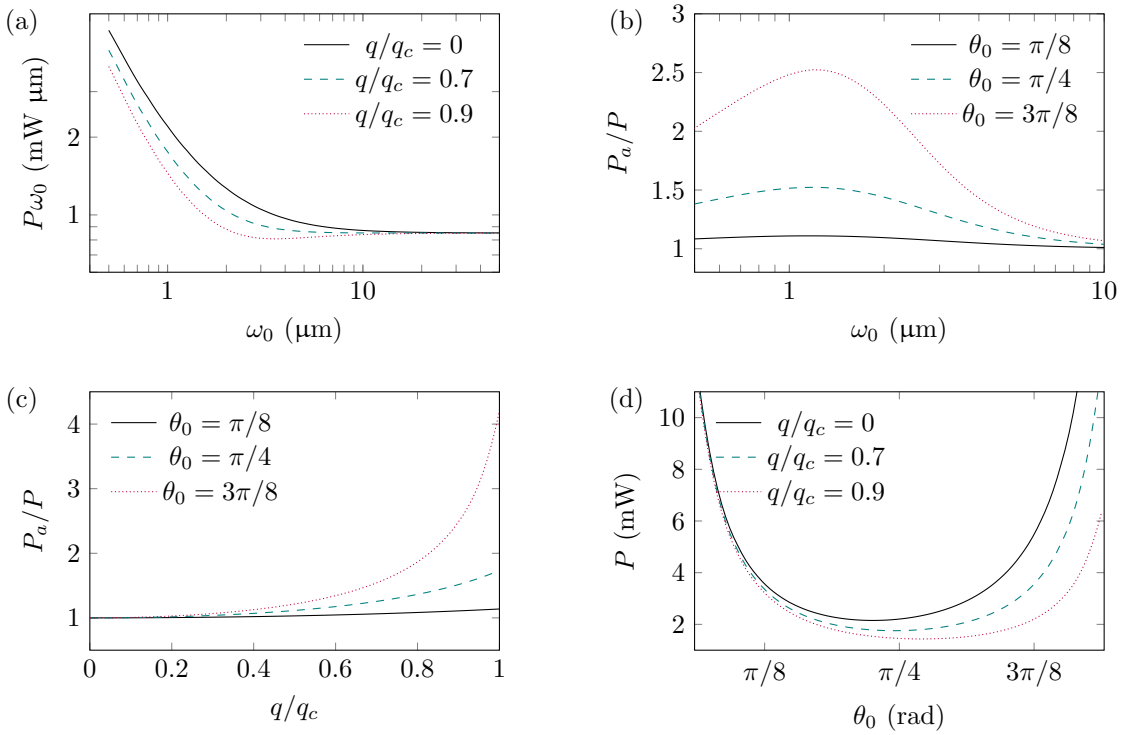

Figure 2. (a) Existence curve $P\omega_0$ of fundamental nematicons as a function of the transverse waist ω_0, with $\theta_0 = \pi/4$. (b) Chirality-enhancement factor P_a/P as a function of ω_0, with P_a (resp., P) the soliton power at $q/q_c = 0$ (resp., $q/q_c = 0.9$). (c) Chirality-enhancement factor $P_a/P[q/q_c]$ as a function of q/q_c, with $\omega_0 = 1$ μm. (d) Soliton power as a function of θ_0, with $\omega_0 = 1$ μm. In (a–d), the elastic anisotropy is neglected ($\kappa_{21} = \kappa_{23} = 1$).

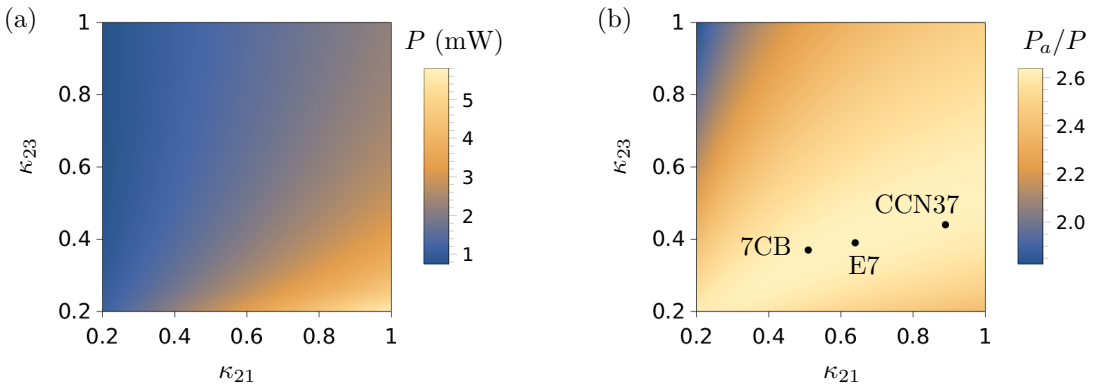

Figure 3. (a) Soliton power as a function of the elastic constants ratio κ_{21} and κ_{23}. (b) Chirality-enhancement factor P_a/P as a function of κ_{21} and κ_{23}. In both graphs, we chose $q/q_c = 0.9$, $\theta_0 = 3\pi/8$ and $\omega_0 = 1$ µm. Since P/P_a is roughly independent of the birefringence, we also plotted in (b) dots associated with common liquid crystals based on measured values of their elastic constants at room temperature.[15,16,18,19]

and material constants defined in Table 1, while varying the parameters ω_0, θ_0, q/q_c, κ_{21} and κ_{23}. We always assumed a fundamental waveguide mode along the x-direction ($m = 1$).

We first focus on the simple case of isotropic elasticity ($\kappa_{21} = \kappa_{23} = 1$). Fig. 2a presents how $P\omega_0$ evolves as a function of the beam waist ω_0. For waists much higher than the sample thickness, one can observe that $P \propto 1/\omega_0$; this scaling is different from the usual case of nematicons unconfined by the sample plates ($P \propto 1/\omega_0^2$) because in our system the extent of the optical field in the x-direction is already fixed by the chosen waveguide mode. Conversely, at waists smaller than the sample thickness, the soliton power typically varies as $1/\omega_0^3$. We emphasize that a soliton with a waist very different from the sample thickness is likely unstable with respect to the modulational instability,[14] and therefore could decompose into an array of solitons in the direction of the highest optical extent (x if $\omega_0 \ll h$, y if $\omega_0 \gg h$). Since analyzing this instability is beyond the scope of this paper, we focus here on the case of intermediate waists comparable to the sample thickness.

Fig. 2a also shows that the soliton power decreases when q/q_c increases, which is fully compatible with the chirality-enhanced LC response already noted in the last section. To better understand this effect, we introduce the *chirality-enhancement factor* P_a/P, where P_a corresponds to the soliton power in achiral media ($q/q_c = 0$). In Fig. 2b, we show how this factor evolves as a function of the beam waist when P is calculated just below the threshold of instability ($q/q_c = 0.9$). As visible, the boost given by chirality is maximal when $\omega_0 \approx 1.2$ µm $\sim h/2$, whatever the value of the far-field director angle θ_0. This is not really surprising, since this condition is equivalent to saying that the typical beam extent in the y-direction should be comparable to the sample thickness, and therefore the cholesteric pitch since $q/q_c = 0.9$. In short, one can expect a relevant role of chirality if twist has sufficiently room to develop inside the disturbed domain defined by the light beam. This is the reason this paper is focused on the case of light strongly confined between the plates of the sample: axisymmetric beams with lateral extent much smaller than the sample thickness (and therefore than the cholesteric pitch) typically exhibit a much weaker chirality-enhancement effect than here, and are thus not too different from achiral nematicons.

Fig. 2c shows the same chirality-enhancement factor as in Fig. 2b for three different values of θ_0, plotted against the rescaled twist q/q_c instead of the beam waist ω_0. Therein, one clearly sees that the higher θ_0 is, the stronger the chirality-enhancement factor is when q/q_c increases—an effect which is also visible in Fig. 2b. This is expected since $\theta_0 = \pi/2$ (far-field director orthogonal to the direction of light propagation) corresponds to the direction of the first unstable Fourier mode just above the threshold of instability q_c, as already noted above. Below the transition, this mode is partially excited by the optical perturbation, but is of course stable since $q < q_c$. As a consequence, the chirality-enhancement effect that our theoretical model and numerical simulations exhibit can be understood as a pre-transitional effect induced by the frustration of our chiral sample, similar to the increased transverse response that one could get from an elongated elastic beam submitted to a normal pressure below the threshold of buckling.

A simple examination of Eq. (23) shows that $P \propto (P/P_a)P_0 \propto (P/P_a)/\sin^2(2\theta)$, which means that although P/P_a (inverse of the chirality-enhancement factor) goes to zero below the threshold of instability when $\theta_0 \to \pi/2$, the actual soliton power will always be > 0, and should even diverge when $\theta_0 \to \pi/2$. This is simply because the amplitude of molecular reorientation goes to zero as the far-field director becomes aligned with the optical field, which implies that it is harder and harder to get a significant nonlinear optical response when $\theta_0 \to \pi/2$, whatever the magnitude of q/q_c. At the end of the story, only the power P matters when trying to generate a soliton, not the enhancement factor P_a/P. Fig. 2d therefore plots the soliton power P as a function of the far-field director angle θ_0 for three different values of q/q_c. This figure shows that in an achiral media, one need a power of ~ 2.2 mW to generate a fundamental soliton when $\theta_0 = \pi/4$, which roughly corresponds to the minimal soliton power across all director angles. As the rescaled spontaneous twist q/q_c increases, the range of far-field director angles that allows to generate a soliton at the same power of ~ 2.2 mW greatly widens. In short, the chirality-enhancement effect that we demonstrate here is also allowing, for a given input power, the generation of solitons along a much wider range of propagation directions than in the achiral case. This effect could find its use for wide-angle steerage of optical solitons in dedicated photonics devices.

Finally, we quickly describe how the soliton power vary when anisotropic elastic constants are taken into account ($\kappa_{21} \neq 1$ and $\kappa_{23} \neq 1$), with fixed typical values for the other parameters (see legend of Fig. 3). Fig. 3a shows the color-coded variations of P with κ_{21} and κ_{23}, and demonstrate that solitons can be generated at the lowest power for a given birefringence when $K_2 \ll K_1$, whatever the value of $\kappa_{23} = K_2/K_3$. This means that a low free energy cost for twist deformation modes is favored by the chirality-enhanced optical solitons studied here. In addition, Fig. 3b shows how the chirality enhancement factor varies with κ_{21} and κ_{23}. This factor is roughly independent of the birefringence, so that one can make an easy comparison between different liquid crystals with given anisotropy of elastic constants. Interestingly, the boost that chirality gives to the nonlinear optical response is roughly maximal for three widely-used liquid crystals (7CB, E7 and CCN-37) indicated by dots in Fig. 3b, which means that one does not need uncommon liquid crystals with pathological Frank elastic constants to observe a significant chirality-enhancement effect.

3.2 General beam propagation simulations of chirality-enhanced solitons

We now describe numerical results obtained with a general scheme that models both light propagation and molecular reorientation in arbitrarily complex birefringent medium, even beyond the linear response considered in our theory. This scheme is very similar to the one described in a previous paper,[10] in that it consists of repeated interleaved beam propagation steps (BPM steps in the following) allowing to propagate the optical field for a given director field, and LC relaxation steps allowing to the calculate the director field for a given distribution of optical field. These steps are repeated until the relative changes of both director and optical field are below $2 \cdot 10^{-5}$. The LC relaxation steps are performed using the gradient-descent method described in Ref.[10] As for the BPM steps, we used the general paraxial formalism described in Ref.[12] since the sample geometry considered here (arbitrarily tilted in-sample-plane director) is more general than the one considered in Ref.[10] (homeotropic director). All calculations were made using the constants defined in Table. 1, $K_2 = 7$ pN, $K_3 = 18$ pN, $\theta_0 = 70°$ and $\omega_0 = 1$ µm. These material constants are associated with the liquid crystal E7 at room temperature.[15,16] In our numerical code, the input optical field is defined by first calculating numerically the fundamental y-polarized waveguide mode along the x-direction ($m = 1$) using the ARPACK++ library, and then multiply this waveguide mode by a Gaussian of waist of ω_0 along the y-direction.

In Fig. 4a, we show the simulated x-averaged intensity of a beam propagating along z with a vanishingly small power (no molecular reorientation); as expected, this beam is linearly diffracting in the y-direction (but stays confined in the x-direction thanks to the negative jump of permittivity at the sample plates). Conversely, we show in Fig. 4b (resp., Fig. 4c) the same propagating beam, but with a nonzero power $P \approx 3.76$ mW and a rescaled spontaneous twist $q/q_c = 0$ (resp., $q = q_c = 0.9$). In both cases, self-focusing is visibly present thanks to the nonlocal reorientation of LC molecules, but only in the chiral case $q/q_c = 0.9$ is the diffraction fully compensated by the nonlinear optical response, thus giving rise to an almost perfectly z-invariant solitonic amplitude profile. This observation is confirmed more quantitatively in Fig. 4d, where we plot the rescaled waist $\omega(z)/\omega_0$ against the propagation distance z for the beams of Fig. 4a–c. Thus, our general (2+1)D nonlinear beam propagation simulations confirm the same chirality-enhancement effect than in our simplified effective (1+1)D theoretical model.

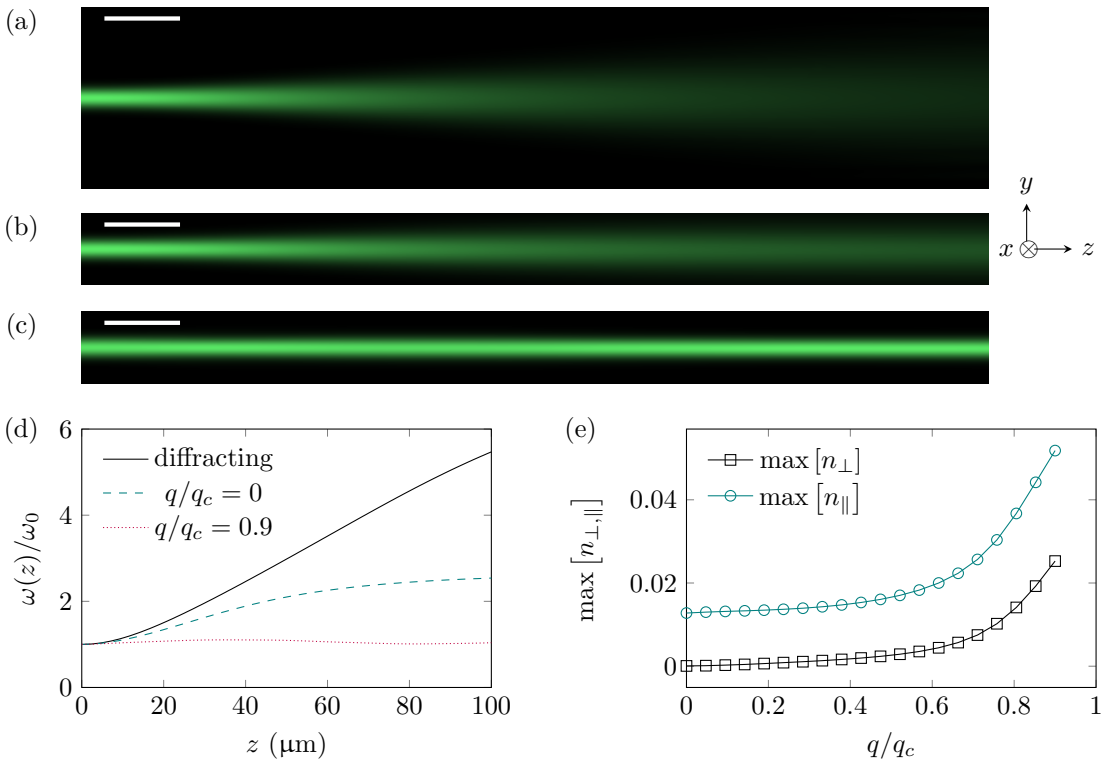

Figure 4. (a) Simulated x-averaged intensity of a diffracting beam ($P = 0$) with $\omega_0 = 1$ µm. (b) Same as (a) with $P = 3.76$ mW and $q/q_c = 0$. (c) Same as (a) with $P = 3.76$ mW and $q/q_c = 0.9$. (d) Rescaled waist $\omega(z)/\omega_0$ as a function of propagation distance z for the beams of (a–c). (d) Maximal director deviations $n_\parallel$ and $n_\perp$ after a propagation distance $z = 200$ µm, as a function of q/q_c.

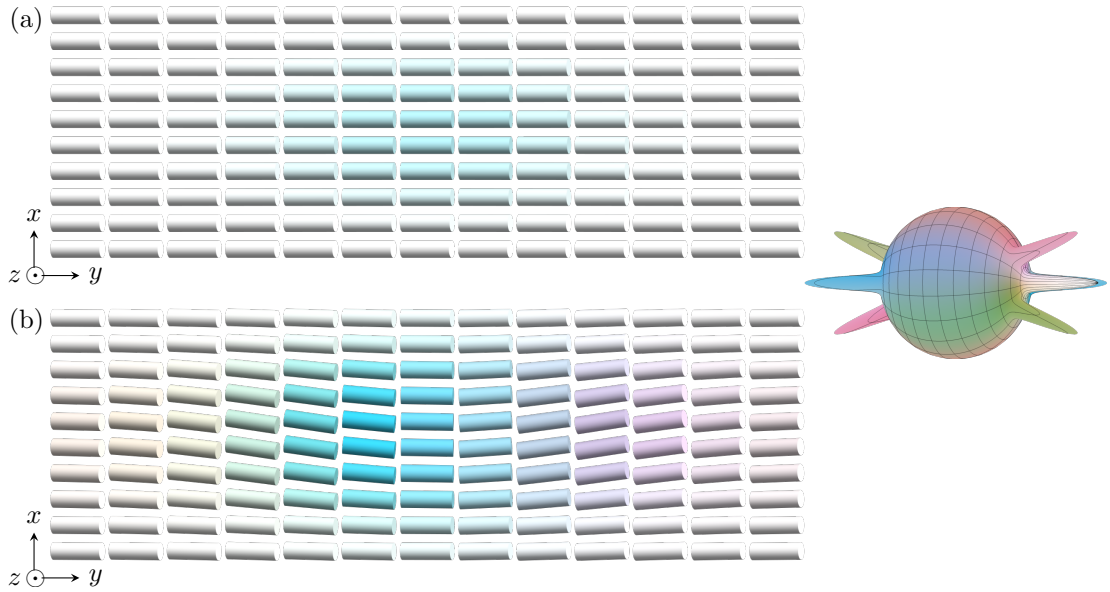

Figure 5. Cylindrical-glyph-based plots of the director field associated with the beam of Fig. 4b (a) and Fig. 4c (b). The cylinders are colored depending on their deviation from the undeformed director field $\boldsymbol{n}_0$ (in white), taking into account the antipodal symmetry $\boldsymbol{n} \to -\boldsymbol{n}$ as shown on the right.

To check how strongly the nonlinear optical response is amplified by chirality, we also plot in Fig. 4e the maximal in-sample-plane and out-of-sample-plane director deviations $n_{\parallel,\perp}$ in the whole computational box as a function of q/q_c. At $q/q_c = 0.9$, $n_\parallel$ is 2.15 times bigger than in the achiral case, which is also exactly what our theoretical model predicts when numerically integrating $\tilde{G}_{\text{eff}}\tilde{J}_{\text{eff}}$. However, we emphasize that the soliton power predicted by our theoretical model ($P \approx 2.66$ mW) is 30 % smaller than the one needed in the general simulation to generate a fundamental soliton at $q/q_c = 0.9$ ($P \approx 3.76$ mW). This quantitative difference is likely due to the approximations made in our model, most notably the fact that the true solitonic amplitude profile is not exactly a waveguide mode times a Gaussian. Nevertheless, our theoretical model is in good qualitative agreement with the simulations and allows to get a precious insight on the variations of the soliton power with all parameters at a much lower computational cost.

We close this section by presenting in Fig. 5 the xy-cross-sections of the director fields associated with the numerically simulated solitons of Fig. 4b–c. The orientation of the director is represented by cylindrical glyphs; deviation angles from the far-field director $\boldsymbol{n}_0$ were amplified by a factor 6 for easier visualization of the director field patterns. We encode each particular director orientation with colors on the S^2 sphere with antipodal symmetry $\boldsymbol{n} \to -\boldsymbol{n}$ (see right of Fig. 5), with white corresponding to the far-field director $\boldsymbol{n}_0$. Blue-like colors indicates a molecular reorientation towards the optical field along y, while red-like and green-like colors indicate an out-of-sample-plane reorientation. In the achiral case (Fig. 5a), the reorientation is fully contained in the yz plane formed by the beam wavevector and polarisation, as expected from classical theory on nematicons.[14] Conversely, in the chiral case (Fig. 5b), twist develops in the y-direction with a nonzero out-of-sample-plane molecular reorientation. The positive sign of the twist can be readily checked by determining the sequence of colors along the y-direction, which is green-blue-red and corresponds to a right-handed circuit around $\boldsymbol{n}_0$ on the S^2 sphere on the right of Fig. 5 (with the thumb oriented along the y-direction).

4. CONCLUSION

We presented a theoretical approach to model the coupling between beam propagation and optically-induced director reorientation in frustrated chiral planar LC. Our model shows that chirality generally amplify the response of the LC to external fields and therefore the nonlinear optical response of the material, thus allowing to generate optical solitons at lower power than in achiral samples. Furthermore, the chiral sample geometry proposed here allows for a wider range of angles between the director and the soliton axis when the input power is fixed. Our theoretical model is only approximate since it relies on an effective average of the wave equation along the sample normal, but is nevertheless in good qualitative agreement with general (2+1)D simulations of optical solitons. To ensure that our results can be easily reused, we created an open-source dataset on the platform Zenodo, which includes the simulated optical solitons as well as Mathematica and python scripts facilitating calculations for our theoretical model. This dataset can be accessed from Ref.[20]

We suggested that the unwound chiral samples necessary to observe the optical solitons described here could be experimentally realized by transitioning the LC from isotropic to cholesteric phase under the action of a strong external field imposing $\boldsymbol{n} = \boldsymbol{n}_0$. For example, one could use a Halbach ring magnet similar to the one of Ref.,[21] which can typically impose a magnetic correlation length as low as 1.5–2 µm for most cyanobiphenyls and should prevent the formation of π-twisted domains when $h > 2$ µm, even for intermediate spontaneous twist $q \in [\pi/(2h), q_c]$ for which these domains are the lowest energy state. First proof-of-concept experiments could be done in samples thicker than the one studied here, since it would simplify the coupling of the input beam through the side of the sample. One could also try to experimentally determine if there is a chirality-enhanced nonlinear optical response in chiral π-twisted LC cells, which are much easier to create than the unwound planar chiral LCs of this paper. Finally, beyond the optical solitons of this study, we believe that the chirality-enhanced response of LC described here could be used to boost the mechanical interaction of optical beams with localized LC patterns or LC colloids,[22] or more generally the optomechanical footprint that light leaves inside LCs,[23] thus showing once again the fundamental role that chirality plays in the properties of soft materials.

APPENDIX A. CALCULATION OF THE EFFECTIVE GREEN FUNCTION

We describe here how to calculate the effective Green function $\tilde{G}_{\text{eff}}$ introduced in the main text. We express it under the following form:

$$\tilde{G}_{\text{eff}} = \frac{\int_{-h/2}^{h/2} \left|\psi^{(m)}(x)\right|^2 \bar{\Gamma}_{\parallel}(x)\ \mathrm{d}x}{\left[\int_{-h/2}^{h/2} \left|\psi^{(m)}(x)\right|^2 k_0 \mathrm{d}x\right]^2}, \tag{25}$$

where $\bar{\Gamma}_{\parallel}$ can be found by solving the following system of differential equations:

$$\begin{pmatrix} \eta_{\perp} q_y^2 - \partial_x^2 & -iq_y\left[\eta_c \partial_x - q\eta_q\right] \\ -iq_y\left[\eta_c \partial_x + q\eta_q\right] & \eta_{\parallel} q_y^2 - \kappa_{21}\partial_x^2 \end{pmatrix} \begin{pmatrix} \bar{\Gamma}_{\perp} \\ \bar{\Gamma}_{\parallel} \end{pmatrix} = \begin{pmatrix} 0 \\ k_0^2 \left|\psi^{(m)}\right|^2 \end{pmatrix}. \tag{26}$$

After enumerating the possible eigenmodes and particular solution for the last equation, we find that the solution for $\bar{\Gamma}_{\parallel}$ can be expressed as:

$$\bar{\Gamma}_{\parallel} = A_{\psi}\left[\left|\psi^{(m)}(x)\right|^2 - \left|\psi^{(m)}\left(\frac{h}{2}\right)\right|^2\right] + \sum_{s=\pm}\left\{A_s\left[\frac{\sinh^2\frac{\alpha_s x}{2} - \sinh^2\frac{\alpha_s h}{4}}{\left(\frac{\alpha_s h}{4}\right)^2}\right] + A_a\sigma_s\frac{\sinh\alpha_s x}{\sinh\frac{\alpha_s h}{2}}\right\}, \tag{27}$$

with $\sigma_{\pm} = \pm 1$. The eigenvalues α_+ and α_- are defined as:

$$\alpha_{\pm} = \sqrt{\left(\frac{\eta_{\parallel} + \eta'_{\perp}}{2}\right) q_y^2 \pm \sqrt{\left(\frac{\eta_{\parallel} - \eta'_{\perp}}{2}\right)^2 q_y^2 + \frac{(\eta_q q q_y)^2}{\kappa_{21}}}}, \tag{28}$$

with $\eta'_{\perp} = \eta_{\perp}/\kappa_{21}$. The solution for $\bar{\Gamma}_{\perp}$ can be found from the first row of Eq. (26), but its expression will not be given here since it is quite lengthy and not useful for the calculation of $\tilde{G}_{\text{eff}}$. By applying Dirichlet boundary conditions for $\bar{\Gamma}_{\perp}$ and expanding the second row of Eq. (26), we find that the coefficient A_{ψ} is exactly given by:

$$A_{\psi} = \frac{k_0^2\left(\eta_{\perp} q_y^2 + \alpha_{\psi}^2\right)}{\left(\eta_{\parallel} q_y^2 + \alpha_{\psi}^2\right)\left(\eta_{\perp} q_y^2 + \kappa_{21}\alpha_{\psi}^2\right) - (\eta_q q q_y)^2}, \tag{29}$$

with $\alpha_{\psi} \equiv 2k_0\xi^{(m)}$, and that the coefficients $A_{\pm}$ and A_a must be solution of the following linear system:

$$A'_{\psi} + \quad \Phi_-^2\cosh(\Phi_+)A_+ + \quad \Phi_+^2\cosh(\Phi_-)A_- \quad = 0, \tag{30}$$

$$\eta_c\left[\zeta_{\psi}\sin(\Phi_{\psi})A_{\psi} + \quad \delta\Phi_-^2\,\mathrm{sinhc}(\Phi_+)A_+ + \quad \delta\Phi_+^2\,\mathrm{sinhc}(\Phi_-)A_-\right] + \quad \frac{\eta_q\Phi_q\left[\Phi_+^2 - \Phi_-^2\right]}{2}A_a \quad = 0, \tag{31}$$

$$\eta_q\Phi_q\left[\zeta_{\psi}\Phi_{\psi}\cos(\Phi_{\psi})A_{\psi} + \quad \delta\Phi_-^2\cosh(\Phi_+)A_+ + \quad \delta\Phi_+^2\cosh(\Phi_-)A_-\right] + \quad \frac{\eta_c\zeta_a}{2}A_a \quad = 0, \tag{32}$$

with $\mathrm{sinhc}(u) \equiv \sinh(u)/u$ and $\mathrm{tanhc}(u) \equiv \tanh(u)/u$. The following quantities were defined to shorten the expression of the linear system:

$$\Phi_{\pm} \equiv \frac{\alpha_{\pm} h}{2}, \qquad \Phi_q \equiv \frac{qh}{2}, \qquad \zeta_{\psi} \equiv \frac{\delta\Phi_+^2\delta\Phi_-^2\Phi_{\psi}}{4\left(\Phi_{\psi}^2 + \eta_{\perp}\Phi_y^2\right)}, \tag{33}$$

$$\Phi_y \equiv \frac{q_y h}{2}, \qquad \delta\Phi_{\pm}^2 \equiv \Phi_{\pm}^2 - \eta_{\perp}\Phi_y^2, \qquad \zeta_a \equiv \eta_{\perp}\Phi_y^2\left[\frac{\delta\Phi_+^2}{\mathrm{tanhc}\ \Phi_-} - \frac{\delta\Phi_-^2}{\mathrm{tanhc}\ \Phi_+}\right], \tag{34}$$

and finally:

$$A'_{\psi} \equiv \frac{\eta'_{\perp}\Phi_y^2 X_c^2 + \Phi_+^2\Phi_-^2\cos(\Phi_{\psi})A_{\psi}}{4}. \tag{35}$$

When $\kappa_{21} = 1$ and $q = 0$, Eqs. (31,32) are undetermined and must be replaced by the conditions $A_a = 0$ and $A_+ = A_-$.

Although the linear system above can be solved analytically, we were not able to sufficiently simplify the lengthy resultant expressions. For this reason, we only performed numerical solving of this system by precalculating all coefficients for a given set of parameters. Once the solution for $A_\pm$ and A_a is obtained, one can finally deduce the effective Green function from Eq. (25,27):

$$\tilde{G}_{\text{eff}} = \frac{h}{X_c^2\left[1+(-1)^{m+1}\text{sinc }\Phi_\psi\right]^2}\left\{\frac{1+2(-1)^m\left[\cos\ \Phi_\psi - \text{sinc }\Phi_\psi\right]-\text{sinc}(2\Phi_\psi)}{8}A_\psi \right. \\ \left. + \sum_{s=\pm}\left[\frac{\text{sinhc }\Phi_s - \cosh\ \Phi_s}{\Phi_s^2} + (-1)^m\frac{\text{sinc }\Phi_\psi\ \cosh\ \Phi_s - \text{sinhc }\Phi_s\ \cos\ \Phi_\psi}{\Phi_s^2+\Phi_\psi^2}\right]A_s\right\}. \tag{36}$$

Note that the coefficient A_a does not appear in the expression above because $\sinh(\alpha_\pm x)\left|\psi^{(m)}(x)\right|^2$ is an odd function of x and therefore yields 0 after integration. Nevertheless, this coefficient is generally nonzero when $\kappa_{21} \neq 1$ and $q \neq 0$ and must be included to accurately model the effect of the anisotropy of elasticity.

ACKNOWLEDGMENTS

The authors warmly thank P. Oswald for a very interesting discussion about the relative stability of unwound and partially twisted director fields in various frustrated chiral sample geometries. The authors acknowledge funding from the ARSS (Javna Agencija za Raziskovalno Dejavnost RS) through Grant No. P1-0099 and from the European Unions Horizon 2020 program through the Marie Skłodowska-Curie Grant Agreement No. 834256 and COST action No. CA17139 (EUTOPIA)

REFERENCES

[1] Karpierz, M. A., "Solitary waves in liquid crystalline waveguides," *Physical Review E* **66**(3) (2002).

[2] Conti, C., Peccianti, M., and Assanto, G., "Observation of Optical Spatial Solitons in a Highly Nonlocal Medium," *Physical Review Letters* **92**(11), 113902 (2004).

[3] Conti, C., Peccianti, M., and Assanto, G., "Route to Nonlocality and Observation of Accessible Solitons," *Physical Review Letters* **91**(7), 073901 (2003).

[4] Peccianti, M., Dyadyusha, A., Kaczmarek, M., and Assanto, G., "Tunable refraction and reflection of self-confined light beams," *Nature Physics* **2**, 737 (2006).

[5] Piccardi, A., Alberucci, A., Bortolozzo, U., Residori, S., and Assanto, G., "Soliton gating and switching in liquid crystal light valve," *Applied Physics Letters* **96**(7), 071104 (2010).

[6] Izdebskaya, Y. V., Desyatnikov, A. S., and Kivshar, Y. S., "Self-Induced Mode Transformation in Nonlocal Nonlinear Media," *Physical Review Letters* **111**(12), 123902 (2013).

[7] Kravets, N., Piccardi, A., Alberucci, A., Buchnev, O., Kaczmarek, M., and Assanto, G., "Bistability with Optical Beams Propagating in a Reorientational Medium," *Physical Review Letters* **113**(2), 023901 (2014).

[8] Perumbilavil, S., Piccardi, A., Barboza, R., Buchnev, O., Kauranen, M., Strangi, G., and Assanto, G., "Beaming random lasers with soliton control," *Nature Communications* **9**(1), 3863 (2018).

[9] Jisha, C. P., Alberucci, A., Beeckman, J., and Nolte, S., "Self-Trapping of Light Using the Pancharatnam-Berry Phase," *Physical Review X* **9**(2), 021051 (2019).

[10] Poy, G., Hess, A. J., Smalyukh, I. I., and Žumer, S., "Chirality-Enhanced Periodic Self-Focusing of Light in Soft Birefringent Media," *Physical Review Letters* **125**(7), 077801 (2020).

[11] Oswald, P. and Pieranski, P., [*Nematic and Cholesteric Liquid Crystals: Concepts and Physical Properties Illustrated by Experiments*], CRC Press (2006).

[12] Poy, G. and Žumer, S., "Physics-based multistep beam propagation in inhomogeneous birefringent media," *Optics Express* **28**(16), 24327 (2020).

[13] Conti, C., Peccianti, M., and Assanto, G., "Spatial solitons and modulational instability in the presence of large birefringence: The case of highly nonlocal liquid crystals," *Physical Review E* **72**(6) (2005).

[14] Assanto, G., ed., [*Nematicons: Spatial Optical Solitons in Nematic Liquid Crystals*], Wiley Series in Pure and Applied Optics, John Wiley & Sons, Hoboken, New Jersey (2013).

[15] Ong, H. L., Schadt, M., and Chang, I. F., "Material Parameters and Intrinsic Optical Bistability in Room Temperature Nematics RO-TN-200, -201, -403, E7, m_1, and m_3," *Molecular Crystals and Liquid Crystals* **132**(1-2), 45–52 (1986).

[16] Brimicombe, P. D., Kischka, C., Elston, S. J., and Raynes, E. P., "Measurement of the twist elastic constant of nematic liquid crystals using pi-cell devices," *Journal of Applied Physics* **101**(4), 043108 (2007).

[17] Ritland, H., "Relation Between Refractive Index and Density of a Glass at Constant Temperature," *J. Am. Ceram. Soc.* **38**(2), 86 (1955).

[18] Karat, P. P. and Madhusudana, N. V., "Elasticity and Orientational Order in Some $4'$- n -Alkyl-4-Cyanobiphenyls: Part II," *Molecular Crystals and Liquid Crystals* **40**(1), 239–245 (1977).

[19] Oswald, P., Poy, G., and Dequidt, A., "Lehmann rotation of twisted bipolar cholesteric droplets: Role of Leslie, Akopyan and Zel'dovich thermomechanical coupling terms of nematodynamics," *Liquid Crystals* **44**(6), 969–988 (2016).

[20] Poy, G., "Dataset for chirality-enhanced optical solitons in planar unwound cholesteric cells," (2021). https://doi.org/10.5281/zenodo.5082286.

[21] Oswald, P., Poy, G., Vittoz, F., and Popa-Nita, V., "Experimental relationship between surface and bulk rotational viscosities in nematic liquid crystals," *Liquid Crystals* **40**(6), 734–744 (2013).

[22] Škarabot, M., Ravnik, M., Babič, D., Osterman, N., Poberaj, I., Žumer, S., Muševič, I., Nych, A., Ognysta, U., and Nazarenko, V., "Laser trapping of low refractive index colloids in a nematic liquid crystal," *Physical Review E* **73**(2), 021705 (2006).

[23] El Ketara, M., Kobayashi, H., and Brasselet, E., "Sensitive vectorial optomechanical footprint of light in soft condensed matter," *Nature Photonics* **15**, 121–124 (2020).